Biomechanical characterization and constitutive modeling of the layer-dissected residual strains and mechanical properties of abdominal porcine aorta

Juan A. Peña [a,b] M. Cilla [b,c,e] Miguel A. Martínez [b,d,e] Estefanía Peña [b,d,e,*]

[a] *Department of Management and Manufacturing Engineering. Faculty of Engineering and Architecture. University of Zaragoza. Spain*

[b] *Applied Mechanics and Bioengineering. Aragón Institute of Engineering Research (I3A). University of Zaragoza. Spain*

[c] *Centro Universitario de la Defensa. Academia General Militar. Zaragoza.Spain*

[d] *Department of Mechanical Engineering. University of Zaragoza. Spain*

[e] *CIBER de Bioingeniería, Biomateriales y Nanomedicina (CIBER-BBN). Zaragoza. Spain*

Abstract

We analyze the residual stresses and mechanical properties of layer-dissected infrarenal abdominal aorta (IAA). We measured the axial pre-stretch and opening angle and performed uniaxial tests to study and compare the mechanical behavior of both intact and layer-dissected porcine IAA samples under physiological loads. Finally, some of the most popular anisotropic hyperelastic constitutive models (GOH, microfiber and four fiber models) were proposed to estimate the mechanical properties of the abdominal aorta by least-square fitting of the recorded in-vitro uniaxial test results.

The results show that the residual stresses are layer dependent. In all cases, we found that the OA in the media layer is lower than in the whole artery, the intima and the adventitia. For the axial pre-stretch, we found that the adventitia and the media were slightly stretched in the environment of the intact arterial strip, whereas the intima appears to be compressed. Regarding the mechanical properties, the media seems to be the softest layer over the whole deformation domain showing high anisotropy, while the intima and adventitia exhibit considerable stiffness and a lower anisotropy response. Finally, all the hyperelastic anisotropic models considered in this study provided a reasonable approximation of the experimental data. The four-fiber model showed the best fitting.

Key words: Infrarenal abdominal aorta, layer separation, residual strains, uniaxial testing, constitutive modeling, elastic properties.

* Corresponding author. Tel.: +34876555233; Fax: +34976762578

Email address: fany@unizar.es (Estefanía Peña).

1 Introduction

Loss of structural integrity of the aorta can result in potentially life threatening aneurysms or dissections with a significant risk of rupture (Sassani et al., 2015a). There is, therefore, a pressing need to understand better the mechanisms underlying the stiffness and structural integrity of central arteries, both healthy and diseased. Healthy arteries are composed of three clearly defined layers. The intima (the innermost layer) consists of a single layer of endothelial cells, a thin basal membrane and a subendothelial layer; the media (the middle layer) is composed of a 3D network of elastin, smooth muscle cells and collagen fibres; and the adventitia (the outer layer) consists of fibroblasts, fibrocytes, ground matrix and thick bundles of collagen fibres (Rhodin, 1980). Given that the arterial wall is a non-homogeneous material, the best approach is to model the heterogeneity of the arterial wall by considering it as a multi-layer structure while incorporating its architecture and its different layers, the intima, media and adventitia (Holzapfel and Ogden, 2010b; Díaz et al., 2021). To the best of the authors' knowledge, the studies by Sommer et al. (2010) on human carotid arteries, Peña et al. (2015) on porcine thoracic descending aortas, Sokolis et al. (2012); Sassani et al. (2015b,a) on thoracic and abdominal aortic aneurysms and Amabili et al. (2019); Amabilii et al. (2020) on human descending thoracic aorta are the only works that present the layer-specific mechanical properties and residual stresses at the same time.

The preferred methodology to describe and reproduce the mechanical behavior of arteries is the definition of a strain energy function (SEF) from which the stress response is derived, see e.g. (Alastrué et al., 2009; Holzapfel et al., 2000; Zullinger et al., 2004; Gasser et al., 2006; Holzapfel and Ogden, 2010a; Sokolis, 2010) and references therein. The response of fibers are typically assumed to be governed by exponential functions (Holzapfel et al., 2000, 2005). However, structurally-motivated material models may provide increased insights into the underlying mechanics and physics of arteries and could overcome this drawback (Weisbecker et al., 2015). The work by Gasser et al. (2006) included structural information in the model by means of the assumption of a fiber orientation following a von Mises distribution function. More recently, models including fiber dispersion from a micro-structurally based approach have been proposed using an axially symmetric von Mises or Bingham orientation distribution function (ODF) around two preferred mean directions (Alastrué et al., 2009) and (Alastrué et al., 2010).

Several experimental studies have been conducted to determine and model the mechanical properties of human (Amabili et al., 2019; Choudhury et al., 2009; Haskett et al., 2010; Kamenskiy et al., 1998; Sokolis, 2015; deGeest et al., 2004; Weisbecker et al., 2012), porcine (Guo and Kassab, 2004; Kim and Baek, 2011; Lillie et al., 2010; Peña et al., 2015, 2018; Silver et al., 2003; Sokolis, 2007; Zeinali-Davarani et al., 2013), murine (Guo and Kassab, 2003) and ovine aortas (Haslach et al., 2011) by means of inflation, uniaxial and biaxial tests. To the best of the author's knowledge the studies by Sassani et al. (2015a) and Weisbecker et al. (2012) are the only ones which analyze the layer-specific uniaxial mechanical properties of abdominal aorta. The elegant work by Sassani et al. (2015a) is the only work that presents the layer-specific mechanical properties and residual stresses simultaneously and analyzes the constitutive modeling for abdominal aorta. A number of candidate constitutive models were analyzed and compared for their efficacy in reproducing the material response of each layer. However they focused on abdominal aortic aneurysms. On the other hand, Weisbecker et al. (2012) conducted uniaxial tension tests on layer-separated human abdominal aortic tissue samples tested up to the supra-physiological loading range to analyze the damage of the tissue. However, in that paper there is no data about the mechanical response over a physiological range or residual strains.

The purpose of the current study was to quantify the axial pre-stretch and opening angle and performed uniaxial tests to study the mechanical behavior of both intact and layer-separated porcine infrarenal abdominal aorta under physiological loads and reported values of constitutive parameters for well-known strain energy functions. Finally, two structural models (Gasser et al., 2006; Baek et al., 2007) and one micro-structural model (Alastrué et al., 2009) were proposed to estimate the mechanical properties of the abdominal aorta by least-square fitting of the recorded in-vitro uniaxial test results.

2 Materials and methods

Seven abdominal porcine aortas were harvested from female pigs approximately 3.5 ± 0.45 months old. The experiments were approved by the Ethical Committee for Animal Research of the University of Zaragoza. The animals were sacrificed under general anesthesia through an intravenous injection of potassium chloride and sodium thiopental, and the infrarenal abdominal aorta (IAA) were harvested. Their *in situ* length was measured, then the specimens were dissected, and their *ex situ* length recorded. The axial stretch λ_z^0, defined as the ratio between the *in situ* and *ex situ* measured lengths, was then computed. After artery harvesting and cleaning, the IAA were kept frozen at -18ºC until testing.

2.1 Experiments

After being defrozen, the samples were preserved Krebs-Ringer solution at 4 [$°C$] until the preparation for testing was carried out. Two 2÷3 [mm] arterial rings and two 5x25 [mm] longitudinal strips were cut. Following the protocol described in Peña et al. (2015), we locate suitable places where the layer separation process can be carried out. One ring and one longitudinal strip were carefully separated with minimal force with the aid of a microscope and using a scalpel, first separating the intima and then the media from the adventitia. Hematoxiline-eosine histological stains were prepared to confirm correct layer separation and that the separation did not induce damage. Samples with a faulty separation process were discarded. For intima, we used a threshold of 3 lamellas to exclude specimens with an incorrect intima-media layer separation. Three measurements at different locations were taken using a Mitutoyo Digimatic micrometer (202 mm^2 of maximum contact area), which held the measurement when the contact force reached a value of 0.5 [N], to measure the length, width and thickness of the samples. The measurements were averaged.

Arterial ring segments (intact and layer-dissected) were arranged in Krebs-Ringer solution (25ºC) in a Petri dish and then cut open by radial cuts. The OA was defined as the angle subtended by the lines connecting the midpoint of the inner circumference with the ends of the ring. The opening angle and the stress free dimensions were measured using ImageJ software after 30 min to fully release the residual stress. The axial stretch with respect to the non-separated strips λ_z^* were also determined, so the total axial residual stretch for each layer could be computed as $\lambda_z^{res} = \lambda_z^0 \lambda_z^*$ (Peña et al., 2015).

Simple tension tests of the circumferential and axial IAA rectangular strips (5x25 [mm]) were performed in a high precision drive Instron Microtester 5548 system using a 10 [N] load cell with a minimal resolution of 0.005 [N]. A non-contact Instron 2663-281 video-extensometer was used to measure the strain during the tests. To avoid specimen drying, we used an ultrasonic humidifier enabling humidity to be maintained during the test. Three loading and unloading stress cycle levels were applied: corresponding to approximately 60, 120 and 240 [kPa] uniaxial stress at 30%/min of strain rate (García et al., 2011) under load control. Five preliminary cycles at all load levels were applied in order to precondition the sample. The engineering stress (first Piola Kirchhoff stress tensor $\mathbf{P}$) in the direction of the stretch was computed as $P_{\theta\theta,zz} = \frac{F_{\theta,z}}{t_{\theta,z} w_{\theta,z}}$, where F is the load registered by the Instron machine and $t_{\theta,z}$ and $w_{\theta,z}$ are the initial thickness and width in circumferential and longitudinal directions respectively.

It was considered helpful to measure the anisotropy of the samples at the estimated physiological stress state in the artery, approximated by a thin tube under a physiological pressure of 120 mmHg (using Laplace's law $\sigma_{\theta\theta} = \frac{Pr}{t}$) that for IAA corresponds to 116 kPa. Anisotropy was analyzed by the difference in longitudinal and circumferential stretches divided by their average value (Kamenskiy et al., 1998).

2.2 *Strain-energy functions*

Only the elastic properties of the tissue were considered, so we take into account only the experimental tests at the second level (120 [kPa]) after preconditioning, i.e. the last curve obtained for that level (Peña et al., 2015).

2.2.1 *Gasser-Ogden-Holzapfel model*

The Gasser-Ogden-Holzapfel (GOH) model proposed by Gasser et al. (2006) as an extension of the model of Holzapfel et al. (2000) by the application of a generalized structure tensor $\mathbf{H} = \kappa\mathbf{1} + (1 - 3\kappa)\mathbf{M}_0$ (where $\mathbf{1}$ is the identity tensor and $\mathbf{M}_0 = \mathbf{m}_0 \otimes \mathbf{m}_0$ is a structure tensor defined using unit vector $\mathbf{m}_0$ specifying the mean orientation of fibers) is considered

$$\Psi = \mu\left(I_1 - 3\right) + \sum_{i=4,6}\left[\frac{k_1}{2k_2}\left(exp\left\{k_2\hat{E}_i\right]\} - 1\right)\right], \tag{1}$$

where $I_1 = tr\bar{\mathbf{C}}$ represents the first invariant of the Cauchy-Green tensor ($\mathbf{C} = \mathbf{F}^T\mathbf{F}$) characterizing the isotropic mechanical response of the elastin (Gundiah et al., 2009; Lillie et al., 2010), $\mathbf{F}$ is the deformation gradient (Spencer, 1971) and

$$\hat{E}_i = \kappa I_1 + (1 - 3\kappa)I_i - 1 \quad i = 4, 6 \tag{2}$$

where

$$I_4 = \lambda_\theta^2\cos^2(\theta) + \lambda_z^2\sin^2(\theta), \qquad I_6 = \lambda_\theta^2\cos^2(-\theta) + \lambda_z^2\sin^2(-\theta). \tag{3}$$

In this equation I_1 represents the first invariant of the Cauchy-Green tensor (Spencer, 1971) characterizing the isotropic mechanical response of the elastin (Gundiah et al., 2009; Lillie et al., 2010), $\mu > 0$, $k_1 > 0$ are stress-like parameters, $k_2 > 0$ and κ are dimensionless. Here, θ is the orientation angle relative to the circumferential direction. $\kappa \in [0, 1/3]$ is a dispersion parameter (the same for each collagen fiber family). When $\kappa = 0$, the model is the same as the one published in Holzapfel et al. (2000), and when $\kappa = 1/3$ it recovers an isotropic potential similar to that used in Demiray (1972).

2.2.2 *Four-Fiber-Family model*

The second constitutive model, called Four Fiber Family (FFF), is a hyperelastic anisotropic model proposed by Baek et al. (2007). The model is used for stress-strain description of human aortas and aneurysms (Ferruzzi et al., 2011; Sassani et al., 2015b). The model represents an elastin-dominated amorphous matrix reinforced by four families of (collagen) fibers (in axial, circumferential and diagonal directions).

$$\Psi = \frac{c}{2}\left(I_1 - 3\right) + \sum_{i=1}^{4} \frac{c_1^i}{4c_2^i}\left[exp\left(c_2^i[I_4^i - 1]^2\right) - 1\right], \tag{4}$$

In this equation $c > 0$, $c_1^i > 0$ are stress-like parameters, $c_2^i > 0$. $I_4^i = \mathbf{M}_0^i \cdot \mathbf{M}_0^i \mathbf{C}$ represents the square of the stretch of the ith-fiber family. The fiber orientations are defined by the unit vectors $\mathbf{M}_0^i$, which depend on angles θ_0^i defined between directions of fiber reinforcement and the circumferential direction. Hence, circumferential and axial fibes are fixed at $\theta_0^1 = 0$ and $\theta_0^2 = 90$, respectively, while the diagonal fibers are accounted for by $\theta_0^3 = -\theta_0^4 = \theta_0$.

2.2.3 *Microfiber model*

Following Alastrué et al. (2010), we consider a microfiber model (microsphere-based model) to account for the dispersion of the collagen fibers around a preferential direction. Consistent with the constrained mixture approach (Humphrey and Rajagopal, 2003), the free energy function takes the form $\Psi = \mu\left(I_1 - 3\right) + \Psi_{\text{coll}}$, where the subscripts *coll* refers to the collagen fibers contribution. Ψ_{coll} is defined as the sum of the contributions of each collagen family of fibrils as

$$\Psi_{\text{coll}} = \sum_{j=1}^{N} \left[\Psi_{\text{coll}}\right]^j = \sum_{j=1}^{N} \langle n\rho\psi_{\text{coll}}\rangle^j = \sum_{j=1}^{N} \frac{1}{4\pi}\int_{\mathbb{U}^2} (n\rho[\psi_{\text{coll}}])^j dA, \tag{5}$$

where N denotes the number of families of collagen fibers, $N = 2$ according to the experimental results of orientation of the collagen fibers (Holzapfel et al., 2000), and applying a discretization to the continuous orientation distribution on the unit sphere $\mathbb{U}^2$, $[\Psi_{\text{coll}}]^j$ corresponds to the expression

$$[\Psi_{\text{coll}}]^j = \sum_{i=1}^{m} n\rho(\mathbf{r}^i; (\lambda^i_{\text{coll}}) \tag{6}$$

where $\mathbf{r}^i$ are the unit vectors associated with the discretization on the microsphere over the unit sphere $\mathbb{U}^2$ and m is the number of discrete orientation vectors (Alastrué et al., 2009). $\lambda^i_{\text{coll}} = \|\mathbf{F} \cdot \mathbf{r}^i\|$ the stretch in $\mathbf{r}^i$ direction and $\psi^i_{\text{coll}}(\lambda^i_{\text{coll}})$ the strain energy function associated with $\mathbf{r}^i$ direction. ρ is the orientation density function (ODF) to take into account the fibrils dispersion (Alastrué et al., 2009). A 3D bi-π-periodic von Mises ODF were considered to the modeling of the IAA (Alastrué et al., 2010). This function is expressed as

$$\rho(\theta) = \rho_1(\theta) + \rho_2(\theta), \tag{7}$$

where $\theta = \arccos(\mathbf{m}.\mathbf{r})$ is the so-called mismatch angle and $\mathbf{m}$ the preferred mean orientation of the collagen distribution, and

$$\rho_i(\theta) = 4\sqrt{\frac{b}{2\pi}}\,\frac{\exp\left(b\left[\cos(2\,\theta) + 1\right]\right)}{\operatorname{erfi}(\sqrt{2\,b})}, \tag{8}$$

where the positive concentration parameter b constitutes a measure of the degree of anisotropy. Moreover, $\operatorname{erfi}(x) = -\,i\operatorname{erf}(x)$ denotes the imaginary error function.

Considering the affine kinematics to define the collagen fiber stretch $\lambda^i_{\text{coll}} = \|\mathbf{t}^i\|$ in the fiber direction $\mathbf{r}^i$, the exponential-like strain energy function proposed by Holzapfel et al. (2000)

was used to deal with the fiber response

$$n\psi^i_{\text{coll}}(\lambda^i_{\text{coll}}) = \frac{c_{1\text{coll}}}{2c_{2\text{coll}}}\left(e^{c_{2\text{coll}}((\lambda^i_{\text{coll}})^2-1)^2}-1\right) \qquad if \qquad \lambda_i \geq 1 \quad \text{otherwise} \quad \psi_{\mathrm{f}\,i}(\lambda_i)=0, \tag{9}$$

since it is usually considered that collagen fibers only affect global mechanical behavior in tensile states (Holzapfel et al., 2000). Finally, $c_{1\text{coll}}$ and $c_{2\text{coll}}$ are stress dimensional and dimensionless material parameters respectively.

2.3 Data fitting

The fitting of the experimental data was developed by using a Nelder and Mead type minimization algorithm (Nelder and Mead, 1965) defining the objective function $\chi^2 = \Sigma_{i=1}^n \left[\left(P_{\theta\theta} - P^{\Psi}_{\theta\theta}\right)^2_i + \left(P_{zz} - P^{\Psi}_{zz}\right)^2_i\right]$ using HyperFit software (www.hyperfit.wz.cz). The tissue was assumed as incompressible (Carew et al., 1968), i.e. $\det(\mathbf{F}) = \lambda_1\lambda_2\lambda_3 = 1$, where $\mathbf{F}$ represents the deformation gradient tensor and λ_i, $i = 1, 2, 3$, the stretches in the principal directions. $P_{\theta\theta}$ and P_{zz} are the First Piola-Kirchhoff (engineering) stress data obtained from the tests, and $P^{\Psi}_{\theta\theta} = \frac{\partial\Psi_{\text{iso}}}{\partial\lambda_\theta}$ and $P^{\Psi} = \frac{\partial\Psi_{\text{iso}}}{\partial\lambda_z}$ are the First Piola-Kirchhoff (engineering) for the ith point for a homogeneous pure uniaxial state Ψ, and n is the number of data points. The coefficient of determination $R^2 \in [0, 1]$ was computed for each fitting where $R^2 \geq 0.85$ typically represents a good fit to the experimental data. Finally, the normalized mean square root error $\varepsilon \in [0, 1]$, $\varepsilon = \frac{\sqrt{\frac{\chi^2}{n-q}}}{\varpi}$, were computed for each fitting. In this equation, $\varpi = \frac{\Sigma_{i=1}^n(\sigma)_i}{n}$ is the mean value of the measured stresses, q is the number of parameters of the SEF, so $n - q$ is the number of degrees of freedom, and μ the mean stress already defined above. $\varepsilon \leq 0.15$ typically represents a good fit to the experimental data.

2.4 Statistics

The Shapiro-Wilk Test was used to test for normal distribution . Welch's t test, with the two-sided significance level of $p<0.05$, was used to test the difference between groups.

3 Results

In 4 layer samples, the layer separation process was not successful, the failure point was reached before the 120 kPa cycle due to damage of the samples or slippage of the tissue was presented. In those cases, a new sample was dissected to have at least one sample in circumferential and longitudinal directions for each layer per animal.

3.1 Experiments

The thickness of the total wall for all samples of the IAA was: 1.06±0.10 [mm] while the thickness of the individual layers was 0.13±0.02 [mm] for the intima, 0.53±0.13 [mm] for the media, and 0.51±0.12 [mm] for the adventitia, see Figure 1.a. The inner diameter of the IAA was 6.52±1.530 [mm] and for each arterial layer, –intima, media, and adventitia–, it was 7.37±0.33 [mm], 7.75±0.52 [mm] and 8.58±0.56 [mm], respectively for all the specimens, see Figure 1.b. The ratio of total wall thickness to inner diameter of all the IAA specimens was 0.18±0.02 and for the intima, media, and adventitia the ratio was 0.02±0.004, 0.07±0.02, and 0.06±0.02, respectively, see Figure 1.c. Finally, the ratio of layer-thickness to total wall thickness was 0.11±0.02 for the intima, for the media 0.38±0.09, and 0.43±0.24 for the adventitia, see Figure 1.d.

[Fig. 1 about here.]

Figure 2.a shows column plots of the opening angle values after 30 min of equilibration in the Krebs-Ringer solution for the IAA corresponding to the rings for the whole artery and the

dissected layers. The OA value for the intact layer was 70.61º±17.11. For the separated layers the values were 138.87º±27.31 for the intima, 40.01±20.58 for the media, and 91.34º±12.34 for the adventitia. The axial *in situ* stretch (λ_z^0) was 1.60±0.06. The column plots in Figure 2.b represent the total pre-stretches (mean values and associated standard deviations) of the IAA axial strips after separation into their three layers. Figure 2.b indicates that the media seems to be slightly stretched in the environment of the intact arterial strip. The total pre-stretch values (λ_z^{res} for the intima, media and adventitia were 1.49±0.08, 1.66±0.07 and 1.59±0.10, respectively. We note that the intima is the shortest of the three layers after separation, indicating that the intima is under compression in the unloaded state.

[Fig. 2 about here.]

Figure 3 shows the mechanical responses of the intact arterial tissue in the circumferential and longitudinal directions. All samples exhibit a pronounced nonlinear mechanical response in both directions with a soft transition from the low stiffness region to the high stiffness portion of the curve. Specimens are stiffer in the circumferential direction than in the longitudinal direction showing remarkable anisotropy.

[Fig. 3 about here.]

Representative mechanical responses of dissected intima, media and adventitia layers obtained from the IAA are shown in Figure 6. Different mechanical behaviors between circumferential and longitudinal directions are clearly depicted for all the layers, see also Table 1. The circumferential curves are stiffer and present, in general, a lower dispersion than the longitudinal ones. The adventitia and intima samples present a tendency to be stiffer than the corresponding media samples in the longitudinal direction, see Table 1, where stretches at 60 kPa and 120 kPa for all the layers are summarized. The intima samples show quasi-isotropic behavior and the lowest pronounced nonlinearity (Figure 6 and Table 1). Welch's t test reveals significant differences ($p < 0.01$) in the anisotropy between whole arteries and dissected layers.

[Fig. 4 about here.]

[Table 1 about here.]

3.2 *Histology*

Transverse histological cuts of the specimens stained with Hematoxiline-eosine are shown in Figure 5. Anatomic separation of the arterial sample into its three layers were checked. For most specimens only a few laminae of the media are still attached to the intima or adventitia.

[Fig. 5 about here.]

3.3 *Data fitting*

Material parameters for the intact arteries and their related intima, media and adventitia samples are summarized in the Tables 2, 3 and 4. The values obtained of ε are very low for all the fitted data clearly demonstrating the goodness of the fitting. All SEFs performed adequately ($\varepsilon < 0.15$) with whole data, but only the four family model afforded proper simulation of the mechanical response for the intima, media and adventitia ($\varepsilon = 0.0468 \pm 0.0165$, $\varepsilon = 0.0502 \pm 0.0350$ and $\varepsilon = 0.0494 \pm 0.0173$, respectively). Less accurate but altogether good simulations were obtained with the GOH and microfiber models.

The GOH dispersion parameter κ was 0.1392 ± 0.0710 for whole artery, 0.2753 ± 0.0245 for the intima layer, 0.1175 ± 0.0776 for the media and 0.2529 ± 0.0678 for the adventitia, showing high dispersion or a more isotropic response for the intima and adventitia. Equivalent results were obtained by the microfiber model where the dispersion parameter b had values of 9.4754 ± 3.0455 for the whole artery, 2.1143 ± 1.2463 for the intima layer, 3.4245 ± 3.3857 for the media and 3.1142 ± 2.8994 for the adventitia. There is no equivalent dispersion parameter for the four family model.

[Table 2 about here.]

[Table 3 about here.]

[Table 4 about here.]

[Fig. 6 about here.]

4 Discussion

In this paper, we analyze the layer-separated residual stresses and mechanical properties of the infrarenal abdominal aorta (IAA). We measured the axial pre-stretch and opening angle and performed uniaxial tests to study and compare the mechanical behavior of both intact and layer-separated porcine IAA samples under physiological loads.

Regarding the geometry and *in situ* pre-stretch, we found that the opening angles for the whole artery and media layer are smaller than for the intima and adventitia layers. In all cases, we found the OA in the media layer is lower than in the whole artery, the intima and the adventitia. These results are comparable with those reported by Stergiopulos et al. (2001) for carotid or Holzapfel et al. (2007) for human aorta where the residual stress on intima and adventitia is "compensated" by the media as a composite. However, Sokolis (2019) obtained a contrary tendency to that obtained in our work; the adventitia and the media-intima layers showed OAs higher than the intact artery for porcine IAA. These differences can be explained by the fact that the experiments of Sokolis (2019) dissected the aorta in two layers: intima-media and adventitia. For the axial pre-stretch, we found that the adventitia and the media were slightly stretched in the environment of the intact arterial strip for each orientation, whereas the intima seems to be compressed. Only the works of Sokolis (2019) provide data for the porcine dissected layer abdominal aorta. They found the intima-media layer compressed and the adventitia stretched. Sokolis et al. (2017) obtained an OA for human abdominal artery between 60° and 160° for young patients (age less than 40 years), as well as diameters around 7 and 7.5 mm and 200 to 250° OA and 8.3 and 8.7 mm diameter for older patients. Our results for porcine abdominal artery without pathologies are similar to those of young human patients although slightly smaller between 60° and 90° of OA and between 6.5 and 8 mm of diameter. There was no data about the axial in situ stretch. Again, the lack of separation between the intima and media layers hinder a comparison with our data. Holzapfel et al. (2007) obtained for human aorta a similar tendency to that presented herein. However, they found axial *in* *situ* stretches for human abdominal aorta of 1.196 which is lower than that obtained by (Hang and Fung, 1995) and that obtained in our work (1.6) for young pigs. This is due to the fact that the axial pre-stretch strongly depends on the age, and the human data of Holzapfel et al. (2007) was obtained for aged patients.

The uniaxial test data show that the media seems to be the softest layer over the whole deformation domain, and that the intima and adventitia exhibit considerable stiffness, particularly in the high loading domain in the longitudinal direction. However, there are no differences in the mechanical response of the whole artery and each layer for the circumferential directions. On basis of these results, a single-layer approach for characterizing the mechanical response of thoracic aorta would be inappropriate. The whole artery and media samples show the most pronounced anisotropy presenting a higher anisotropic index than the intima and adventitia. The apparent lower anisotropy for the intima, may be caused by the organization of the collagen fibers as pointed out by Polzer et al. (2015). Regarding the layer specific mechanical properties, Holzapfel et al. (2005) found similar results for the human coronary artery. However, they found that the intima and adventitia of coronaries show the most pronounced nonlinearity and isotropy similarly to our IAA data. Finally, Amabili et al. (2019) is the only work that present simultaneously the layer-specific mechanical properties and residual stresses for the human thoracic descending aorta. They reported that the intima layer is generally the stiffest, with insignificant differences in behavior for the axial and circumferential.

In this work, we study a series of constitutive models, some with a phenomenological approach and others which are micro-structural and physically-oriented, describing the features of the arterial wall with greater accuracy. The fitted GOH, four-family and microfiber hyperelastic models are presented in Tables 2, 3 and 4, respectively. The stress-stretch curves obtained were fitted with the hyperelastic anisotropic models providing a reasonable approximation to the experimental data. The GOH model (Holzapfel et al., 2000) and the microfiber model (Alastrué et al., 2010) were not able to capture the uniaxial properties of the intact and media layer of IAA over a lower range of uniaxial deformations, showing the best prediction at high stretches. The RMSE of the GOH model and the micro-structured model with the von Mises ODF function were similar for all positions. The errors of the fitting procedure might be explained by the coupling effect (overparameterization) of the constitutive model, and different combinations of material parameters may have similar stress-strain response. This nonlinear coupling has resulted in identification difficulties in the optimization-based fitting approaches. The lowest values of RMSE were obtained for the four family of fibers for the whole artery and each separated layer. This is due to the fact that in the four-family fibers model, where the number of fiber families increases from 2 to 4, there is significant improvement in the goodness-of-fit between the model predictions and experimental results. However, if we want to use the histological (microstructural) data obtained, we cannot correlate the measurements with the four-fiber family model.

The findings of this study should be interpreted within the context of its limitations. Regarding the experimental analysis, a small number of tissue samples (n=7) were investigated. Another relevant limitation relates to the use of uniaxial tension tests for separated layers instead of biaxial tests. As pointed out by Holzapfel et al. (2005), an anatomic separation of arteries into their tissue components in young samples is difficult, even impossible for square samples such as we needed for the biaxial tests. Also, dog-bone samples were not possible to obtain and rectangular samples with a 5:1 length-width ratio were used in the uniaxial tests. The aortas were kept frozen at -20°C until testing. No significant difference was found between the elastic modulus of porcine aortic tissue before and after freezing at -20°C and it was unaffected by the storage time (O'Leary et al., 2014). With regard to the material fitting, only data in the range used to fit the model is theoretically predictable (until 120 kPa). The orientation of collagen fibers was not included by a probability density function and the dispersion parameters κ and b and the mean fiber orientation angle are estimated during the fitting procedure, so it should be analyzed as phenomenological parameter.

The results obtained correspond to young samples without pathologies whose results are equivalent to those obtained by Sokolis et al. (2017) for human abdominal aorta from young patients. Obtaining human samples from young patients without pathology is difficult. Therefore, data on the behavior of the aorta before the onset of pathologies can help to understand how and why, for example, aneurysms, aortic dissection or atheromatous plaques might develop.

5 Conclusions

There are three main findings from this study: first, the residual stresses are layer dependent. The intima circumferentially opened by 138º on average, becoming quasi-flat, whereas the media opened similarly to the intact wall. In all cases, we found that the OA in the media layer is lower than in the whole artery, intima and adventitia. For the axial pre-stretch, we found that the adventitia and the media were slightly stretched in the environment of the intact arterial strip for each orientation, whereas the intima seems to be compressed. Second, the media seems to be the softest layer over the whole deformation domain showing high anisotropy. The intima and adventitia exhibit considerable stiffness and a lower anisotropy response. Finally, all the hyperelastic anisotropic models considered in this study provided a reasonable approximation of the experimental data, the four-fiber model showing the best fitting.

6 Acknowledgments

The authors gratefully acknowledge research support from the Spanish Ministry of Science and Technology through research projects PID2019-107517RB-I00, the regional Government of Aragón support for the funding of the research project T24-20R, and the University of Zaragoza for the use of the Servicio General de Apoyo a la Investigación-SAI. Part of the work was performed by the ICTS “NANBIOSIS” specifically by the Tissue & Scaffold Characterization Unit (U13), of the CIBER in Bioengineering, Biomaterials & Nanomedicne (CIBER-BBN at the University of Zaragoza). CIBER Actions are financed by the Instituto de Salud Carlos III with assistance from the European Regional Development Fund.

7 Conflict of interest

None.

References

Alastrué, V., Martínez, M. A., Doblaré, M., Menzel, A., 2009. Anisotropic micro-sphere-based finite elasticity applied to blood vessel modelling. J Mech Phys Solids 57, 178–203.

Alastrué, V., Saez, P., Martínez, M. A., Doblaré, M., 2010. On the use of bingham statistical distribution in microsphere-based constitutive models for arterial tissue. Mech Res Commun 37, 700–706.

Amabili, M., Balasubramanian, P., Bozzo, I., Breslavsky, I. D., Ferraria, G., 2019. Layer-specific hyperelastic and viscoelastic characterization of human descending thoracic aortas. J Mech Behav Biomed 99, 27–46.

Amabilii, M., Arena, G. O., Balasubramanian, P., Breslavsky, I. D., Cartier, R., Ferrari, G., Holzapfel, G. A., Kassab, A., Mongrain, 2020. Biomechanical characterization of a chronic type a dissected human aorta. J Biomech 110, 109978.

Baek, S., Gleason, R. L., Rajagopal, K. R., Humphrey, J. D., 2007. Theory of small on large: potential utility in computations of fluid-solid interactions in arteries. Comp Meth Appl Mech Eng 196, 3070–3078.

Carew, T. E., Vaishnav, R. N., Patel, D. J., 1968. Compressibility of the arterial wall. Circ Res 23, 61–86.

Choudhury, N., Bouchot, O., Rouleau, L., Tremblay, D., Cartier, R., Butany, J., Mongrain, R., Leask, R. L., 2009. Local mechanical and structural properties of healthy and diseased human ascending aorta tissue. Cardiovasc Pathol 18, 83–91.

Díaz, C., Peña, J. A., Martínez, M. A., Peña, E., 2021. Unraveling the multilayer mechanical response of aorta using layer-specific residual stresses and experimental properties. J Mech Behav Biomed 113, 104070 1-15.

deGeest, J. P. V., Sacks, M. S., Vorp, D. A., 2004. Age dependency of the biaxial biomechanical behavior of human abdominal aorta. ASME J Biomech Eng 126, 815.

Demiray, H., 1972. A note on the elasticity of soft biological tissues. J Biomech 5, 309–311.

Ferruzzi, J., Vorp, D. A., Humphrey, J. D., 2011. On constitutive descriptors of the biaxial mechanical behaviour of human abdominal aorta and aneurysms. J R Soc Interface 8, 435–450.

García, A., Peña, E., Laborda, A., Lostalé, F., de Gregorio, M. A., Doblaré, M., Martínez, M. A., 2011. Experimental study and constitutive modelling of the passive mechanical properties of the porcine carotid artery and its relation to histological analysis. Implications in animal cardiovascular device trials. Med Eng Phys 33, 665–676.

García, A., Peña, E., Martínez, M. A., 2012. Influence of geometrical parameters on radial force during self-expanding stent deployment. Application for a variable radial stiffness stent. J Mech Behav Biomed 10, 166–175.

Gasser, T. C., Ogden, R. W., Holzapfel, G. A., 2006. Hyperelastic modelling of arterial layers with distributed collagen fibre orientations. J R Soc Interface 3, 15–35.

Gundiah, N., Ratcliffe, M. B., Pruitt, L. A., 2009. The biomechanics of arterial elastin. J Mech Behav Biomed Mater 2, 288–296.

Guo, X., Kassab, G. S., 2003. Variation of mechanical properties along the length of the aorta in C57bl/6 mice. Am J Physiol Heart Circ Physiol 285, H2614–H2622.

Guo, X., Kassab, G. S., 2004. Distribution of stress and strain along the porcine aorta and coronary arterial tree. Am J Physiol Heart Circ Physiol 286, H2361–H2368.

Hang, H. C., Fung, Y. C., 1995. Longitudinal strain of canine and porcine aortas. J Biomech 28, 637–641.

Haskett, D., Johnson, G., Zhou, A., Utzinger, U., Geest, J. V., 2010. Microstructural and biomechanical alterations of the human aorta as a function of age and location. Biomechan Model Mechanobiol 9, 725–736.

Haslach, H. W., Riley, P., Molotsky, A., 2011. The influence of medial substructures on rupture in bovine aortase. Cardiovascular Engineering and Technology 2, 372–387.

Holzapfel, G. A., Gasser, C. T., Sommer, G., Regitnig, P., 2005. Determination of the layer-specific mechanical properties of human coronary arteries with non-atherosclerotic intimal thickening, and related constitutive modelling. Am J Physiol Heart Circ Physiol 289, H2048–H2058.

Holzapfel, G. A., Gasser, T. C., Ogden, R. W., 2000. A new constitutive framework for arterial wall mechanics and a comparative study of material models. J Elasticity 61, 1–48.

Holzapfel, G. A., Ogden, R. W., 2010a. Constitutive modelling of arteries. Phil Trans R Soc A 466, 1551–1597.

Holzapfel, G. A., Ogden, R. W., 2010b. Modelling the layer-specific 3d residual stresses in arteries, with an application to the human aorta. J R Soc Interface 7, 787–799.

Holzapfel, G. A., Sommer, G., Auer, M., Regitnig, P., Ogden, R. W., 2007. Layer-specific 3d residual deformations of human aortas with non-atherosclerotic intimal thickening. Ann Biomed Eng 35, 530–545.

Humphrey, J. D., 1995. Mechanics of the arterial wall: Review and directions. Crit Rev Biomed Eng 23, 1–162.

Humphrey, J. D., Rajagopal, K. R., 2003. A constrained mixture model for arterial adaptations to a sustained step change in blood flow. Biomech Model Mechanobiol 2, 109–126.

Kamenskiy, A. V., Dzenis, Y. A., Jaffar-Kazmi, S. A., Pemberton, M. A., Pipinos, I. I., Phillips, N. Y., Herber, K., Woodford, T., Bowen, R. E., Lomneth, C. S., MacTaggart, J. N., 1998. Biaxial mechanical properties of the human thoracic and abdominal aorta, common carotid, subclavian, renal and common iliac arteries. Biomech Model Mechanobiol 13, 1341–1359.

Kim, J., Baek, S., 2011. Circumferential variations of mechanical behavior of the porcine thoracic aorta during inflation test. J Biomech 44, 1941–1947.

Lillie, M. A., Shadwick, R. E., Gosline, J. M., 2010. Mechanical anisotropy of inflated elastic tissue from the pig aorta. J Biomech 43, 2070–2078.

Nelder, J. A., Mead, R., 1965. A simplex method for function minimization. Computer J 7, 308–313.

Nolan, D. R., McGarry, J. P., 2016. On the Compressibility of Arterial Tissue. Ann Biomed Eng 44, 993–1007.

O'Leary, S. A., Doyle, B. J., McGloughlin, T. M., 2014. The impact of long term freezing on the mechanical properties of porcine aortic tissue. J Mech Behav Biomed 37, 165–173.

Peña, J. A., Corral, V., Martínez, M. A., Peña, E., 2018. Over length quantification of the multiaxial mechanical properties of the ascending, descending and abdominal aorta using Digital Image Correlation. J Mech Behav Biomed 77, 434–445.

Peña, J. A., Martínez, M. A., Peña, E., 2015. Layer-specific residual deformations and uniaxial and biaxial mechanical properties of thoracic porcine aorta. J Mech Behav Biomed 50, 55–69.

Polzer, S., Gasser, T. C., Novak, K., Mana, V., Tichy, M., Skacel, P., Bursa, J., 2015. Structure-based constitutive model can accurately predict planar biaxial properties of aortic wall tissue.

Acta Biomater 14, 133–145.

Rhodin, J. A. G., 1980. Architecture of the vessel wall, Handbook of Physiology, The Cardiovascular System, vol. 2. American Physiological Society, Bethesda, MD.

Sassani, S. G., Kakisis, J., Tsangaris, S., Sokolis, D. P., 2015a. Layer-dependent wall properties of abdominal aortic aneurysms: Experimental study and material characterization. J Mech Behav Biomed 49, 141–161.

Sassani, S. G., Tsangaris, S., Sokolis, D. P., 2015b. Layer- and region-specific material characterization of ascending thoracic aortic aneurysms by microstructure-based models. J Biomech 48, 3757–3765.

Sherifova, S., Holzapfel, G. A., 2020. Biochemomechanics of the thoracic aorta in health and disease. Prog Biomed Eng 99, 1–17.

Silver, F. H., Snowhill, P. B., Foran, D. J., 2003. Mechanical behavior of vessel wall: A comparative study of aorta, vena cava, and carotid artery. Ann Biomed Eng 31, 793–803.

Sokolis, D. P., 2007. Passive mechanical properties and structure of the aorta: segmental analysis. Acta Physiol 190, 277–289.

Sokolis, D. P., 2010. A passive strain-energy function for elastic and muscular arteries: correlation of material parameters with histological data. Med Biol Eng Comput 48, 507–518.

Sokolis, D. P., 2015. Effects of aneurysm on the directional, regional, and layer distribution of residual strains in ascending thoracic aorta. J Mech Behav Biomed 46, 229–243.

Sokolis, D. P., 2019. Regional distribution of layer-specific circumferential residual deformations and opening angles in the porcine aorta. J Biomech 96, 106335 1–9.

Sokolis, D. P., Kritharis, E. P., Iliopoulos, D. C., 2012. Effect of layer heterogeneity on the biomechanical properties of ascending thoracic aortic aneurysms. Med Biol Eng Comput 50, 1227–1237.

Sokolis, D. P., Savvab, G. D., Papadodimac, S. A., Kourkoulis, S. K., 2017. Regional distribution of circumferential residual strains in the human aorta according to age and gender. J Mech Behav Biomed 67, 87–100.

Sommer, G., Regitnig, P., KÃ¶ltringer, L., Holzapfel, G. A., 2010. Biaxial mechanical properties of intact and layer-dissected human carotid arteries at physiological and supraphysiological loadings. Am J Physiol Heart Circ Physiol 298, H898–912.

Spencer, A. J. M., 1971. Theory of Invariants. In: Continuum Physics. Academic Press, New York, pp. 239–253.

Stergiopulos, N., VulliÃ©moz, S., Rachev, A., Meister, J. J., Greenwald, S., 2001. Assessing the homogeneity of the elastic properties and composition of the pig aortic media. J Vasc Res 38, 237–246.

Weisbecker, H., Pierce, D. M., Regitnig, P., Holzapfel, G. A., 2012. Layer-specific damage experiments and modeling of human thoracic and abdominal aortas with non-atherosclerotic intimal thickening. J Mech Behav Biomed 12, 93–106.

Weisbecker, H., Unterberger, M. J., Holzapfel, G. A., 2015. Constitutive modelling of arteries considering fibre recruitment and three-dimensional fibre distribution. J R Soc Interface 12, 20150111.

Zeinali-Davarani, S., Chow, M.-J., Turcotte, R. L., Zhang, Y., 2013. Characterization of Biaxial Mechanical Behavior of Porcine Aorta under Gradual Elastin Degradation. Ann Biomed Eng 41, 1528–1538.

Zullinger, M., Rachev, A., Stergiopulos, N., 2004. A constitutive formulation of arterial mechanics including vascular smooth muscle tone. Am J Physiol Heart Circ Physiol 287, H1335–H1343.

List of Tables

	λ_θ^{120}	λ_z^{120}	A^{120}	λ_θ^{60}	λ_z^{60}	A^{60}
Whole artery	1.19±0.04	1.36±0.08	0.16±0.03	1.14±0.04	1.33±0.05	0.16±0.026
Intima	1.17±0.07	1.27±0.04	0.09±0.05	1.12±0.04	1.24±0.03	0.10±0.03
Media	1.16±0.04	1.47±0.08	0.24±0.05	1.12±0.04	1.37±0.05	0.19±0.04
Adventitia	1.18±0.06	1.37±0.08	0.15±0.02	1.14±0.04	1.31±0.06	0.14±0.03

Table 1
Circumferential and longitudinal stretches and anisotropy measurements corresponding to 60 kPa and 120 kPa during uniaxial tests. Values are presented as Average±Standard Deviation

Specimen	μ	k_1	k_2	θ	κ	R^2	ε
Whole artery							
I	12.6365	458.7309	673.4996	28.83	0.2752	0.9928	0.0479
II	20.9022	982.9519	708.2242	37.46	0.1379	0.9972	0.03062
III	16.7504	134.7933	70.1169	38.52	0.1264	0.9984	0.02318
IV	10.9810	401.0243	43.1162	39.15	0.0566	0.9992	0.0164
V	29.3678	5.8513	300.6832	34.19	0.2136	0.9844	0.0725
VI	17.9142	349.8984	227.4454	36.73	0.1518	0.9977	0.0257
VII	18.8423	403.6538	0.1615	39.69	0.1152	0.9951	0.0395
Mean	17.3934	213.3840	76.9163	36.1818	0.1392	0.9950	0.0328
SD	6.0233	308.4709	294.1968	3.7924	0.0710	0.0051	0.0190
Mean curve	11.8467	1578.1744	33.1316	39.78	0.0636	0.9926	0.0501
Intima							
I	5.1226	853.8510	211.3070	37.21	0.2484	0.9979	0.0392
II	27.0706	7302.9946	6.9407	6.58	0.3083	0.9877	0.0568
III	11.6378	1525.2551	0.0019	37.07	0.2866	0.9868	0.1033
IV	13.6154	1008.4663	22.0936	37.63	0.2765	0.9671	0.1053
V	8.2341	1217.5817	2.98	15.96	0.2910	0.9398	0.1381
VI	13.0162	22.4826	1176.3743	31.85	0.2386	0.9979	0.0261
VII	0.0105	6449.9160	9.8333	26.41	0.2843	0.9754	0.1196
Mean	4.2423	1078.1611	8.0136	15.0681	0.2753	0.9788	0.0724
SD	8.4865	2950.3424	435.3566	15.4724	0.0245	0.0206	0.0430
Mean curve	6.9257	2846.3490	15.4171	7.33	0.1281	0.9849	0.0653
Media							
I	21.8548	762.9170	7.6170	10.31	0.1175	0.9959	0.0372
II	19.7914	1760.7891	1.2631	36.66	0.0700	0.9927	0.0453
III	17.9965	82.2915	57.7442	38.39	0.0732	0.9881	0.0636
IV	8.5614	331.6519	23.0200	38.44	0.0634	0.9868	0.1421
V	33.3931	34.2622	257.6528	5.87	0.2666	0.98024	0.0791
VI	11.1638	828.1872	10.4041	25.70	0.2072	0.9850	0.1398
VII	7.1638	1289.8882	10.4207	10.96	0.1465	0.9884	0.0610
Mean	15.0877	388.7532	16.6668	12.71	0.1175	0.9882	0.0722
SD	9.1559	638.8697	92.3459	16.4324	0.0776	0.0051	0.0430
Mean curve	26.8563	326.4881	144.4521	16.04	0.1091	0.9911	0.0539
Adventitia							
I	13.7889	877.5483	876.1438	5.04	0.3037	0.9960	0.0363
II	12.5737	5811.7885	17.4556	36.83	0.1144	0.9930	0.0485
III	26.06651	690.6917	41.9081	4.1411	0.2952	0.9946	0.0408
IV	28.1246	597.0324	0.9927	5.84	0.3010	0.9938	0.0443
V	20.0771	166.5962	98.4039	7.95	0.2984	0.9763	0.0880
VI	1.9299	703.9918	74.4546	20.55	0.2751	0.9473	0.1305
VII	8.8685	1758.2219	167.7915	9.54	0.2614	0.984881	0.0673
Mean	12.3442	887.4973	50.0084	9.5026	0.2529	0.9836	0.0589
SD	9.4019	1954.7365	310.9273	11.9393	0.0678	0.0175	0.0340
Mean curve	7.9832	1297.9849	35.7531	11.53	0.3004	0.9932	0.0477

Table 2
Material constants of GOH model (Gasser et al., 2006) obtained for the IAA curves. Constants μ and k_1 in kPa, θ in degrees, k_2, κ and ε dimensionless.

Specimen	c	c_1^1	c_2^1	c_1^2	c_2^2	$c_1^{3,4}$	$c_2^{3,4}$	θ_0	R^2	ε
Whole artery										
I	34.7544	0.4398	11.6530	32.2330	24.6783	0.0506	7.6554	6.99	0.9933	0.0469
II	66.2017	0.6106	9.3837	126.9770	25.9115	0.0395	0.001	1.28	0.9954	0.0362
III	42.7063	2.3646	2.6128	40.4117	0.7826	1.8748	14.7557	12.20	0.9928	0.0490
IV	31.0096	4.4856	1.9824	41.9580	5.9160	1.9446	7.9652	5.72	0.9965	0.03268
V	33.3510	7.2875	1.7555	0.4914	1.5480	2.6395	15.3836	8.93	0.9950	0.0388
VI	43.1379	3.2313	3.6625	40.3492	17.5084	1.6489	21.6301	5.21	0.9981	0.0242
VII	40.2375	6.7574	7.3470	89.6690	27.2213	0.9401	0.1710	12.05	0.9984	0.0228
Mean	40.4239	2.3959	4.2903	27.6445	8.0466	0.6054	1.7546	6.1947	0.9956	0.0345
SD	11.8163	2.7367	3.9678	41.7251	11.7877	0.9951	8.0853	3.9200	0.0022	0.0102
Mean curve	39.6333	4.1275	3.6540	34.1404	13.5602	1.7503	19.8894	8.02	0.9978	0.0265
Intima										
I	27.3095	6.5057	6.8864	43.0056	12.4125	1.2055	14.8318	8.93	0.9968	0.0328
II	79.2891	12.3243	10.6707	177.7176	28.44958	0.0124	9.9304	0	0.9881	0.0554
III	39.4479	10.6809	6.3330	95.4495	1.1390	1.6924	9.1107	6.41	0.9978	0.0267
IV	47.8856	7.2929	5.4621	55.1281	2.6780	1.6846	8.3388	10.82	0.9940	0.0441
V	39.6084	4.2185	6.2471	79.9296	1.9043	1.3278	10.4852	11.17	0.9858	0.0691
VI	39.8955	7.3424	4.7460	113.7596	20.5791	0.0038	11.2351	2.34	0.9931	0.0483
VII	45.8204	4.7734	13.9839	196.2964	29.0005	0.1271	1.2142	5.78	0.9808	0.0690
Mean	43.5301	7.1154	7.2510	95.3740	7.4078	0.2229	7.6970	1.9125	0.9909	0.0468
SD	16.2330	2.9607	3.3332	58.6674	12.3762	0.7852	4.1329	4.2120	0.0062	0.0165
Mean curve	40.7983	6.7224	7.4419	115.8015	5.7599	0.0246	3.0275	14.32	0.9982	0.0245
Media										
I	66.2919	2.9928	2.6876	87.3955	9.3524	0.0012	80.7890	8.25	0.9601	0.1164
II	49.6283	6.1010	2.2243	164.3806	10.9468	0.8753	12.5586	4.12	0.9881	0.0620
III	21.783466	12.0235	0.9418	58.31692	1.5201	1.1960	22.4120	20.79	0.9947	0.0393
IV	32.4433	9.9442	0.86423	9.1471	0.1198	5.6519	12.2345	6.81	0.9964	0.0334
V	58.8459	1.8615	1.3428	0.001	0.001	0.3691	47.8567	17.88	0.9718	0.0931
VI	0.1131	28.2814	0.2878	176.4606	14.4930	2.7854	4.6957	15.41	0.9991	0.0161
VII	41.65416	4.3507	4.2678	115.0859	9.3625	1.4912	7.8380	6.47	0.9902	0.0567
Mean	18.1329	6.5184	1.3465	14.8012	1.1418	0.5243	17.4365	9.7834	0.9857	0.0502
SD	22.7654	9.1099	1.3642	69.7998	5.8839	1.9321	27.8103	6.5133	0.0144	0.0350
Mean curve	36.2677	9.29595	1.1888	56.2004	10.8995	2.1084	0.6052	14.78	0.9969	0.0320
Adventitia										
I	41.7246	0.8141	11.4910	27.7764	23.6147	1.7719	49.8519	3.95	0.9985	0.02191
II	49.3751	0.8230	11.5591	28.9208	30.7391	1.8411	55.2051	6.35	0.9925	0.0438
III	57.5362	4.4357	2.4567	87.7237	1.2325	1.6370	17.4169	13.90	0.9842	0.0601
IV	77.7697	1.0317	0.5027	44.2300	2.1136	2.5457	49.0579	44.06	0.9816	0.0742
V	36.7046	1.1449	2.9021	35.9578	0.001	2.4020	29.4106	29.79	0.9943	0.0439
VI	19.3277	0.35499	4.87739	71.8832	6.57867	11.40906	0.2442	23.20	0.98759	0.0638
VII	54.1546	0.0761	15.5743	60.8469	23.4894	2.0797	2.28349	30.19	0.9893	0.0595
Mean	44.6564	0.7143	4.4790	46.7793	2.2503	2.5867	12.1267	16.4105	0.9897	0.0494
SD	18.2846	1.4582	5.7534	23.0239	12.9298	3.5544	23.0897	14.4409	0.0059	0.0173
Mean curve	16.5409	15.5141	2.2653	22.3355	2.6090	43.3966	6.4583	11.45	0.9971	0.0293

Table 3
Material constants of the FFF model (Baek et al., 2007) obtained for the IAA curves. Constants c and c_1^i in kPa, α_0 in degrees, c_2^i and ε dimensionless.

Specimen	μ	k_1	k_2	θ	b	R^2	ε
Whole artery							
I	54.9964	11.4754	31.8141	17.60	7.6169	0.9689	0.0981
II	55.0442	149.0229	20.5088	28.95	10.0469	0.9804	0.0761
III	40.5664	45.738	10.1622	35.09	15.5046	0.9818	0.0776
IV	40.3181	42.8590	8.5568	31.39	10.9163	0.98614	0.0680
V	63.8841	6.2323	10.6527	18.33	6.4819	0.9709	0.1652
VI	57.5288	61.5486	21.8151	30.93	7.558	0.9918	0.0970
VII	64.0294	93.9274	30.8552	30.79	10.8074	0.9932	0.0998
Mean	52.9380	38.2951	16.9791	26.7484	9.4754	0.9818	0.0936
SD	9.8327	49.6811	9.7598	6.8250	3.0455	0.0095	0.0324
Mean curve 54.3857	32.7026	11.4646	22.91	5.9280	0.9613	0.1122	
Intima							
I	55.0961	17.1556	18.2956	20.77	3.8044	0.9956	0.0627
II	49.7575	201.0553	12.5575	5.75	1.7426	0.9916	0.0895
III	59.6252	42.2675	7.3476	4.53	0.7741	0.9920	0.1130
IV	36.4593	58.8701	4.8751	24.63	1.1116	0.9791	0.0839
V	12.5659	89.2209	4.2606	35.95	2.8082	0.9518	0.1115
VI	69.0247	66.9910	12.3834	6.83	3.8044	0.9914	0.0926
VII	30.1694	117.7335	24.0989	18.59	3.0994	0.9971	0.0654
Mean	39.7189	66.9666	10.0650	12.9422	2.1143	0.9854	0.0864
SD	19.4068	60.5444	7.2890	11.6834	1.2463	0.0160	0.0199
Mean curve	19.6922	97.2772	7.3289	11.45	1.4101	0.9984	0.0231
Media							
I	1.5901	179.8450	1.2064	8.76	1.4333	0.9936	0.0322
II	1.091	219.0568	1.2825	24.26	2.5102	0.9581	0.0958
III	2.4181	76.8744	1.2900	9.59	1.3415	0.9342	0.1196
IV	72.1454	1.8812	15.2560	10.08	5.1965	0.9211	0.1563
V	25.4308	503.0956	2.0039	28.15	6.7839	0.9750	0.1595
VI	25.2593	313.0571	2.9081	26.43	3.0510	0.9856	0.0609
VII	1.3220	598.1179	3.8508	37.01	10.6384	0.9963	0.0352
Mean	5.9272	127.1298	2.5407	17.7978	3.4245	0.9659	0.0793
SD	26.1861	217.4690	5.0732	11.1486	3.3857	0.0295	0.0535
Mean curve	1.6386	463.7468	1.0060	27.34	7.8665	0.9650	0.0931
Adventitia							
I	61.5855	18.2281	25.6480	10.2943	4.8062	0.9639	0.1107
II	10.7132	156.5842	11.1898	37.98	9.9076	0.9859	0.08519
III	25.4911	100.16145	1.5610	24.78	2.0010	0.9953	0.0545
IV	14.4963	110.6977	0.6517	29.73	1.5385	0.9919	0.0498
V	21.9789	27.7524	3.7357	21.71	2.9484	0.9970	0.0305
VI	7.9750	59.3600	4.4763	24.98	2.6208	0.9890	0.055
VII	0.2204	90.6244	10.8757	1.54	2.5080	0.9717	0.0979
Mean	9.9148	64.6583	4.7316	15.7513	3.1142	0.9849	0.0636
SD	20.0621	48.8139	8.7111	12.1530	2.8994	0.0125	0.0291
Mean curve	11.3712	88.8978	3.6571	14.78	1.8019	0.9863	0.06198

Table 4
Material constants of the microfiber model (Alastrué et al., 2010) obtained for the IAA curves. Constants μ and k_1 in kPa, k_2, θ in degrees, b and ε dimensionless.

List of Figures

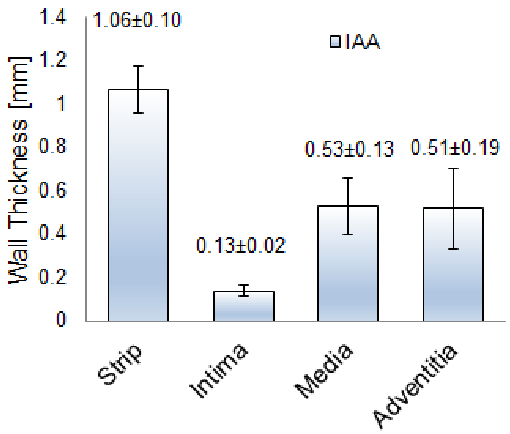

(a) Wall Thickness

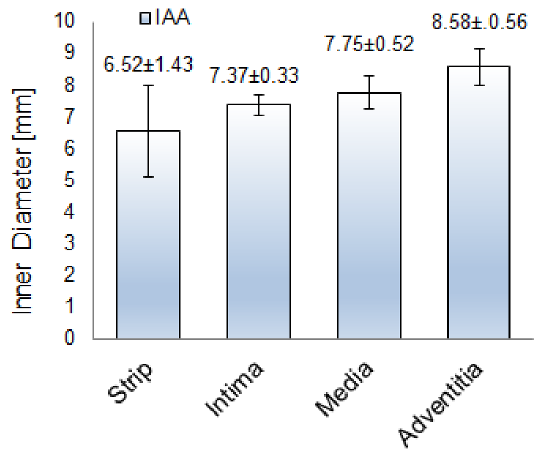

(b) Inner Diameter

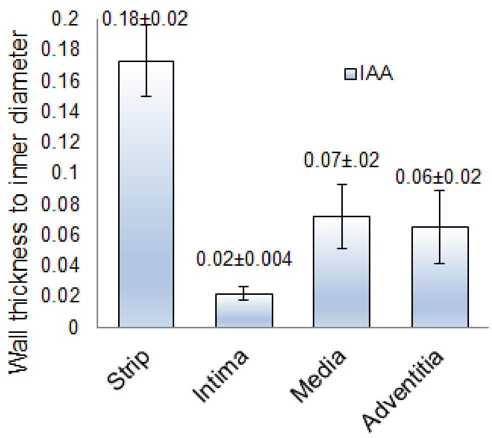

(c) Total wall thickness to inner diameter

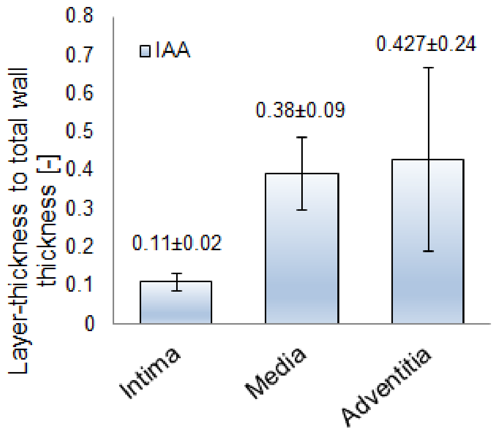

(d) Layer-thickness to total wall thickness

Fig. 1. Column plots of the thickness [mm], inner diameter [mm], ratio of total wall thickness to inner diameter [-] and ratio of layer-thickness to total wall thickness [-] of the IAA samples and the corresponding separated layers (intima, media and adventitia) after 30 min of equilibration. The error bars represent standard deviations.

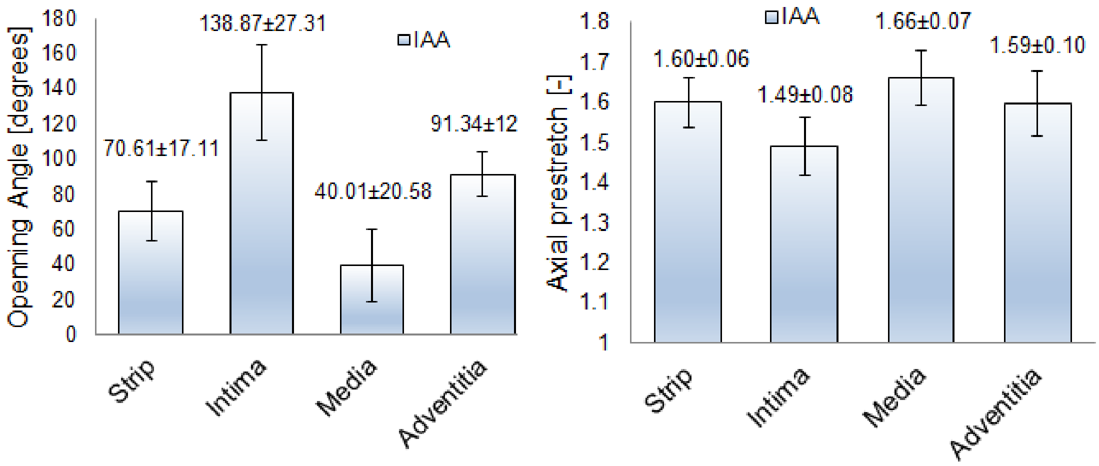

(a) Opening Angle (b) Axial Prestretch

Fig. 2. Column plots of the opening angle [○] and axial prestretch [-] of the IAA samples and the corresponding separated layers (intima, media and adventitia) after 30 min of equilibration. The error bars represent standard deviations.

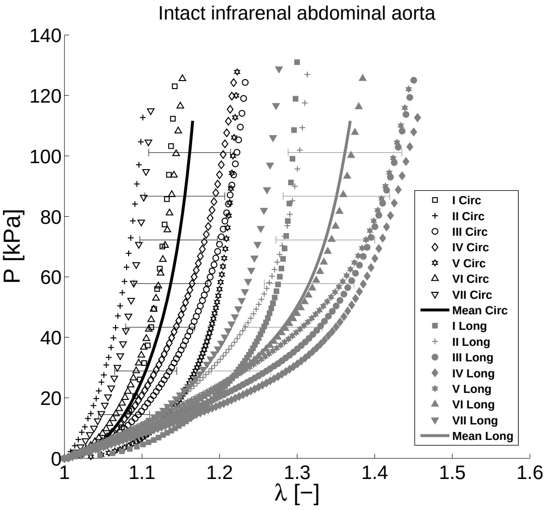

Fig. 3. Uniaxial tensile stress-stretch curves for intact samples I-VII of IAA. Black lines are circumferential directions and grey curves are longitudinal directions. Solid lines are mean curves of experimental data.

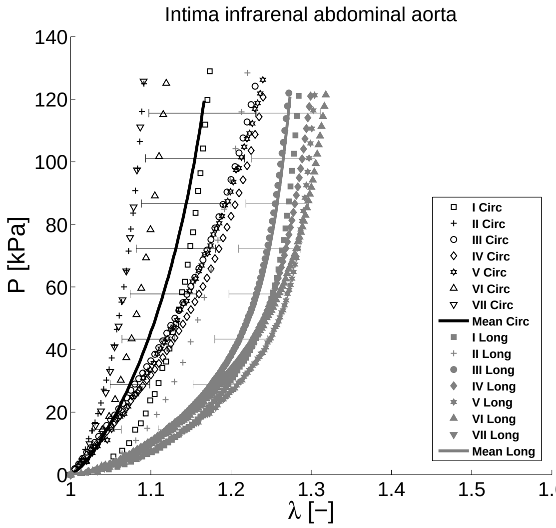

(a) Intima

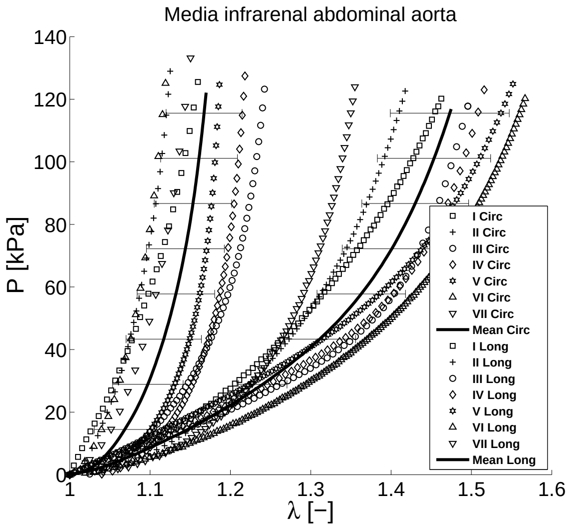

(b) Media

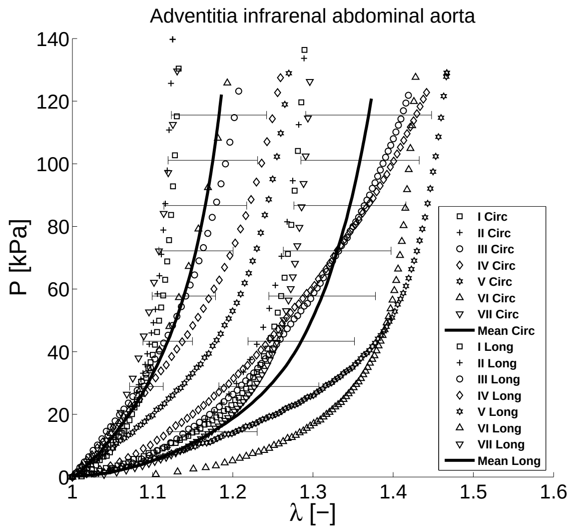

(c) Adventitia

Fig. 4. Uniaxial tensile stress-stretch curves for layer-dissected samples I-VII of IAA. Black lines are circumferential directions and grey curves are longitudinal directions. Solid lines are mean curves of experimental data.

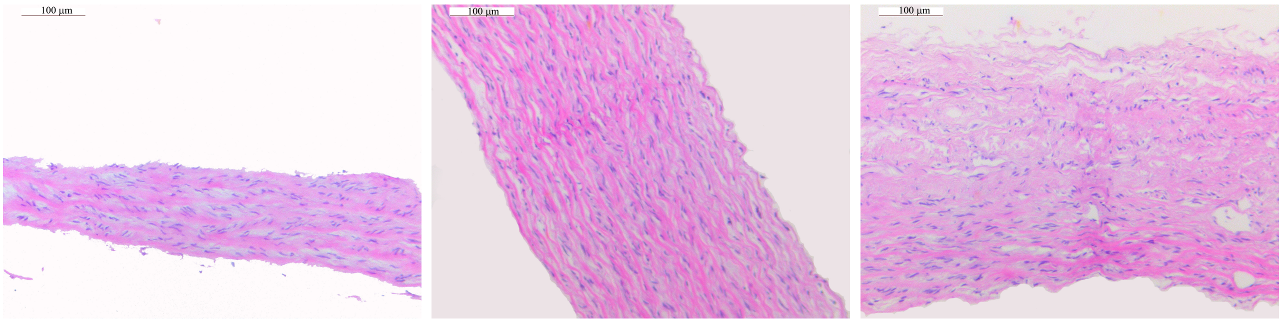

(a) Intima (b) Media (c) Adventitia

Fig. 5. Hematoxylin-and-eosin-stained sections 5 μm from wall layers after anatomic separation of the IAA. Bar measure 100 μm

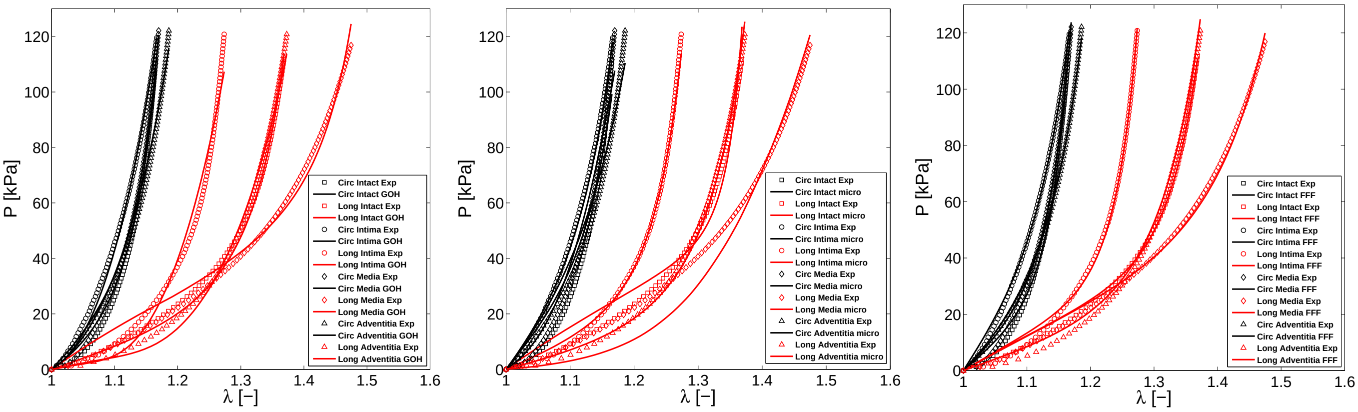

(a) GOH model (b) Microfiber model (c) FFF model

Fig. 6. Mean uniaxial tensile IAA stress-stretch and simulation results with the proposed constitutive models. a) Gasser-Ogden-Holzapfel model (Gasser et al., 2006), b) Microfiber model (Alastrué et al., 2009) and c) Four-Fiber-Family model (Baek et al., 2007).